

# Sheet-Beam Geometry for In-Vivo Fluorescent X-Ray CT: Proof-of-Concept Experiment in Molecular Imaging

Qingkai Huo, Tetsuya Yuasa, Takao Akatsuka

*Yamagata University, Yonezawa, Yamagata, 992-8510 Japan*

Tohoru Takeda, Jin Wu, Thet-Thet-Lwin

*University of Tsukuba, Tsukuba, Ibaraki, 305-8575 Japan*

Kazuyuki Hyodo

*KEK, Tsukuba, Ibaraki, 305-0801 Japan*

F. Avraham Dilmanian

*Brookhaven National Laboratory, Upton, NY, 11973 USA*

E-Mail: [yuasa@yz.yamagata-u.ac.jp](mailto:yuasa@yz.yamagata-u.ac.jp)

Abstract: We propose a fluorescent x-ray computed tomography (CT) method using an array of detectors with an incident sheet-beam, aimed at providing molecular imaging with high sensitivity and good spatial resolution. In this study, we prove the feasibility of this concept and investigate its imaging properties including spatial and contrast resolutions and quantitiveness, by imaging an acrylic phantom and a normal mouse brain, using a preliminary imaging system with monochromatic synchrotron x rays.

**Keywords:** Fluorescent x ray, computed tomography, molecular imaging, synchrotron radiation

Fluorescent x-ray computed tomography (FXCT), which combines x-ray fluorescence measurements and tomographic reconstruction algorithms, allows the distribution of trace elements within samples to be investigated with high sensitivity and at high spatial resolution, in a non-destructive and non-invasive manner [1-10]. In addition, the use of synchrotron radiation (SR) allows FXCT to obtain resolutions of  $\mu\text{m}$  [6]. FXCT has been an indispensable tool for microscopic analysis in both material and biomedical science. Molecular imaging using a non-radioactive imaging-agent, such as iodine, is also of potential use in medicine and pharmacology, where the visualization of various disease processes in small animals is used to elucidate their pathophysiology and in drug discovery. For this purpose, positron emission tomography (PET) or single photon emission computed tomography (SPECT) have been developed in small animals, despite their low spatial resolution. Although SR-FXCT allows sub-millimeter resolution, this approach is hampered by the long measurement time required, as conventional FXCT is based on the first generation type of computed tomography (CT), which acquires a set of projections by translational and rotational scans using pencil-beam geometry [4-10]. In order to complete the measurements during the course of anesthesia, the number of projections and the data acquisition time for each data point need to be reduced, resulting in a reduction in image quality. Thus, just a few

slices can be obtained for in vivo imaging of a rat head, while under anesthesia. Therefore, conventional FXCT cannot substitute for PET or SPECT, which can obtain 3-D tomographic images.

The long measurement time of conventional FXCT, based on pencil-beam geometry, is due to sequential data acquisition, and for faster measurements, simultaneous or parallel acquisition of a single projection is indispensable. We therefore adopted sheet-beam geometry with a linear detector array. Fig. 1 shows a schematic diagram of the proposed imaging geometry. An incident monochromatic sheet beam, where photon fluxes are parallel to one another and are linearly polarized in a plane containing the cross-section of interest, impinges on the object to cover the width of the object cross-section. Imaging agents, such as iodine, are thus excited and isotropically emit x-ray fluorescence photons on de-excitation. A linear array of detectors, where  $n$  solid state detectors operating in a photon-counting mode with energy resolution are equally spaced, is positioned perpendicular to the beam propagation in the plane of polarization for the lowest Compton-scatter contribution in the spectrum, due to the property of linear polarization [4]. A long slit-like collimator is installed in front of each detector element in order to restrict the regions emitting x-ray fluorescence incident to the detective surface, and to reduce the amount of stray radiation being detected. For

example, the  $i$ th detector in Fig. 1 ideally detects just the fluorescent photons on line RS.

Concerning the measurement by the  $i$ th detector along path  $P \rightarrow Q \rightarrow S$  in Fig. 1, the measurement process is divided into three steps: **Step 1**) Attenuation of incident flux rate during the propagation from points P to Q, **Step 2**) isotropic emission of x-ray fluorescence photons at point Q, whose quantity is proportional to both the incident flux rate and the iodine quantity at point Q, and **Step 3**) attenuation of fluorescent flux rate toward the detector during the propagation from points Q to S. As each point on line RS is similarly subject to the above process, the number of fluorescent photons detected by the  $i$ th detector is obtained by integrating the contributions from all the points on RS. As a result, the detector array from the 1st to the  $n$ th detectors simultaneously acquires projection data in a direction perpendicular to the beam propagation. Translational scans are therefore no longer required during the collection of a set of projections, though some translational scans may still be necessary to obtain a single complete projection, because each detector is partitioned by a collimator and no data are obtained at the collimator walls. The overall measurement time will still be drastically reduced, as a set of projections can be collected through rotational and fewer translational scans. Apart from **Step 1**, the measurement process based on the sheet-beam geometry is the same as

that for SPECT. We can reconstruct a tomographic image from a system of algebraic equations representing the above processes [4,5,9,10].

In order to prove the concept of this imaging protocol, we constructed a preliminary imaging system for simulating the proposed imaging geometry using a single SSD using the BLNE-5A bending-magnet beamline (6.5 GeV) at KEK, Japan. The photon flux rate in front of the object was approximately  $9.3 \times 10^7$  photons/mm<sup>2</sup>/s for a beam current of 40 mA. The FXCT system consisted of a silicon (220) double crystal monochromator to tune the incident energy to 37 keV above the iodine K-edge of 33.2 keV, an x-ray slit system to shape a sheet beam of 1.5 cm  $\times$  0.5 mm, scanning tables for subject-positioning, an HPGe detector operating in photon-counting mode to detect emitted fluorescent photons, and a PIN-diode detector to monitor incident intensity. The long slit-like Pb collimator was placed in front of the detective surface of the HPGe detector. The collimator had four parameters:  $L$ ,  $W$ ,  $H$ , and  $S$  were the collimator length, slit width, slit height, and air gap, respectively. The HPGe detector with the long collimator to collimate the emitted fluorescent flux was fixed and the object was scanned through the positioning stages, controlled by a PC, in the following sequence: the object was first translationally scanned along the incident direction  $n$  times at a step of  $\Delta x$ , and then rotationally scanned at a step of  $\Delta \theta$ . Although the

projection data were sequentially acquired by the preliminary imaging system, the set of data obtained after completion of the whole scan was the same as that acquired by the proposed imaging method using the detector array.

Firstly, we evaluated the spatial and contrast resolution, and quantitiveness by imaging a physical phantom using the preliminary system. The acrylic cylindrical phantom was 10 mm in diameter and included three axial channels of 3 mm in diameter, filled with iodine at three different concentrations. Projections were generated from the net counts within the energy window centered at the iodine  $K_{\alpha}$  line (28.3 keV), after subtracting the multiple scatter background. Fig. 2 (a) shows an FXCT image of the physical phantom filled with iodine solution at 50  $\mu\text{g/ml}$ , 100  $\mu\text{g/ml}$ , and 200  $\mu\text{g/ml}$ , generated by the proposed method. The measurement parameters were as follows:  $W = 0.25$  mm,  $H = 1.0$  mm,  $L = 100$  mm,  $S = 0.25$  mm,  $\Delta x = 0.25$  mm, and  $\Delta\theta = 2$  degrees. The measurement time for a single data point was 10 s and the dead-time rate was less than 10%. Three circles corresponding to the regions including the iodine solution are successfully delineated. Fig. 2 (b) shows the differential profile at the yellow line drawn in Fig. 2 (a). The spatial resolution defined by the FWHM of the differential profile peak is approximately 0.35 mm. We imaged the phantom whilst changing the iodine concentrations, and then obtained the average reconstructed values for the regions of

interest and added the iodine values to the reconstructed images. Fig. 2 (c) shows the relationship between the average reconstructed values and the actual iodine concentrations, which demonstrates a satisfactory linear relationship. The dotted line represents the standard deviation of the background noise in the reconstructed images. The minimum detectable iodine concentration, which can be calculated from the intersection of the calibration line and the dotted line representing background noise, is approximately 5.0  $\mu\text{g/ml}$ . From the above results, we conclude that FXCT is suitable for the imaging of rat brains *in vivo*, as our previous FXCT results, based on pencil-beam geometry, determined the iodine concentration in a mouse brain *in vivo* to be a few tens of  $\mu\text{g/ml}$ .

We imaged a normal mouse brain *ex vivo* to confirm the suitability of this technique for biomedical imaging. A mouse brain was excised 15 minutes after an intravenous injection of the non-radioactive ligand, N-isopropyl-p-[ $^{127}\text{I}$ ] iodine amphetamine ( $^{127}\text{I}$ -IMP) at about 0.05 mg/ml, and then fixed in formalin and imaged under the following conditions:  $W = 0.25$  mm,  $H = 1.0$  mm,  $L = 50$  mm,  $S = 0.25$  mm,  $\Delta x = 0.25$  mm, and  $\Delta\theta = 2$  degrees. The measurement time for a single data point was 12 seconds, and the dead-time rate was less than 10%. Fig. 3 shows the FXCT image of the excised mouse brain. The cortex and thalamus can be identified anatomically, and

the iodine content of the brain is estimated at about 20.0  $\mu\text{g}/\text{ml}$  on average, based on the calibration line.

If the detector elements are 2-dimensionally arrayed, we can obtain a 3-D CT image by piling up the 2-D tomographic images. In addition, if the CCD camera is placed downstream of the object, we can simultaneously obtain a transmission image which can provide auxiliary data for attenuation correction and morphological information. The proposed FXCT can therefore simultaneously obtain both morphological and functional information, while PET/CT requires separate measurements to obtain the two kinds of images.

### **Acknowledgment**

This research was partially supported by a Grant-In-Aid for Scientific Research (#09780789, #20500385, #19390313) from the Japanese Ministry of Education, Science and Culture, and performed under the auspices of KEK (2007G643).

## References

- [1] P. Boisseau, *Hyperfine Interactions* 33, 283 (1987).
- [2] J.P. Hogan, *IEEE Trans Nucl. Sci.* 38, 1721 (1991).
- [3] R. Cesareo, *NIM A* 277, 669 (1989).
- [4] T. Yuasa, M. Akiba, T. Takeda, M. Kazama, A. Hoshino, Y. Watanabe, K. Hyodo, F.A. Dilmanian, T. Akatsuka, Y. Itai, *IEEE Trans. Nucl. Sci.* 44, 54 (1997).
- [5] G.F. Rust, J. Weigelt, *IEEE Trans. Nucl. Sci.* 45, 75 (1998).
- [6] A. Simionovici, M. Chukalina, C. Schroer, M. Drakopoulos, A. Snigirev, I. Snigireva, B. Lengeler, K. Janssens, F. Adams, *IEEE Trans. Nucl. Sci.* 47, 2736 (2000).
- [7] T. Takeda, A. Momose, Q.W. Yu, T. Yuasa, F.A. Dilmanian, T. Akatsuka, Y. Itai, *Cell. Mol. Biol.* 46, 1077 (2000).
- [8] C. Schroer, *Appl. Phys. Lett.* 79, 1912 (2001).
- [9] B. Golosio, A. Simionovici, A. Somogyi, L. Lemelle, M. Chukalina, A. Brunetti, J. *Appl. Phys.* 94, 145 (2003).
- [10] P.J. Riviere, P.A. Vargas, *IEEE Trans. Med. Imag.* 25, 1117 (2006).

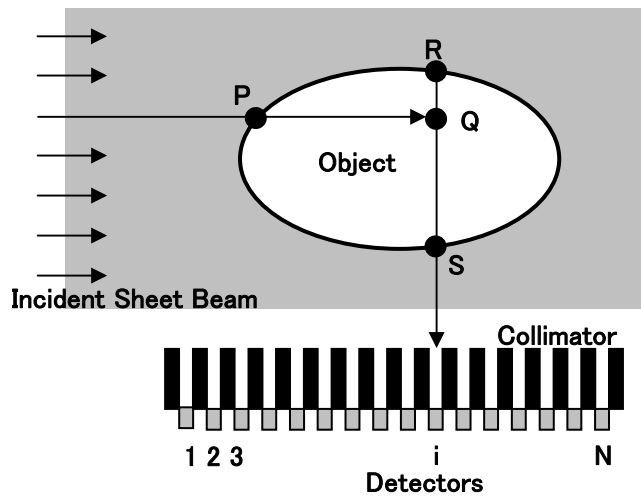
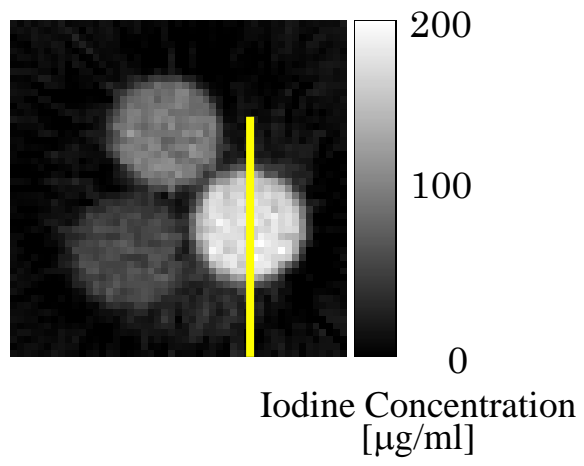
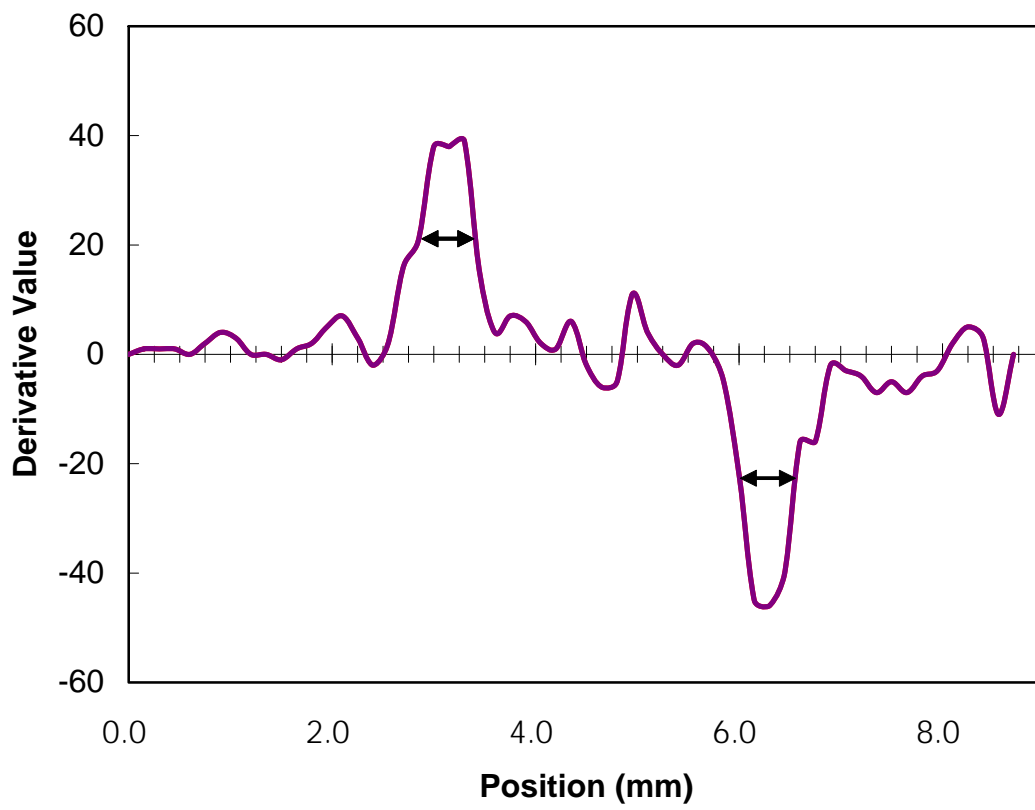


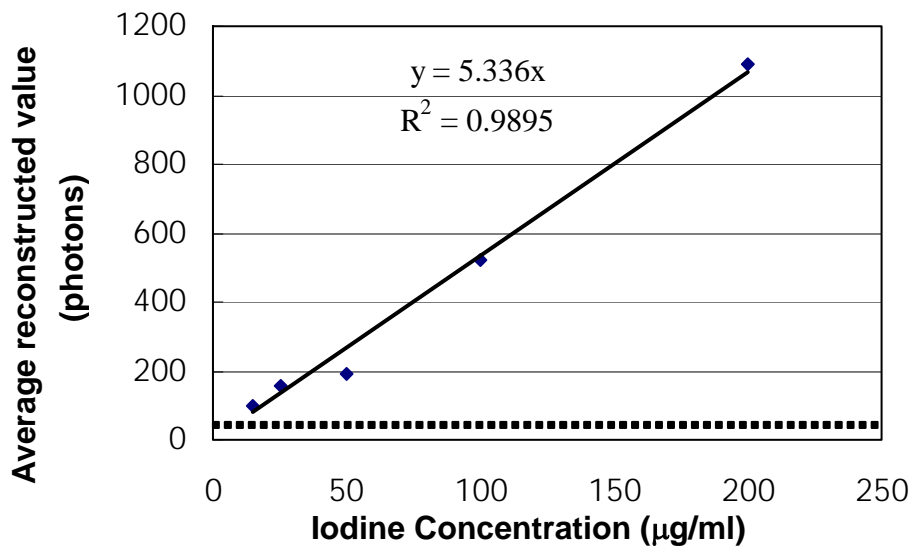
**Fig. 1** Schematic diagram of FXCT imaging geometry using sheet-beam and linear detector arrays.



(a)



(b)



(c)

**Fig. 2** CT measurement of a physical phantom: (a) an FXCT image, (b) the differential profile at the yellow line drawn in Fig. 2 (a), and (c) the relationship between the average reconstructed value and the actual iodine concentration. Correlation coefficient,  $R^2$ , is about 0.99.

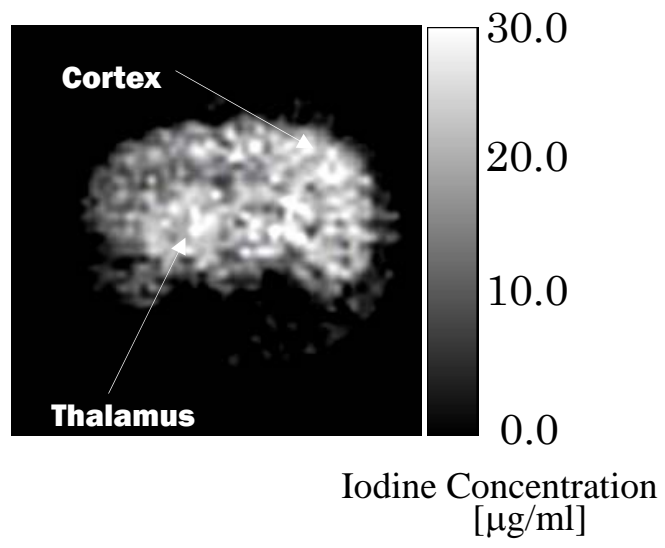


**Fig. 3** Ex vivo FXCT image of a normal mouse brain